Journal of Applied Engineering and Technological Science
Vol 7(2) 2026: 1177-1201

NOISE REDUCTION OF MOTION AND EMG ARTIFACTS IN HOLTER ECG USING IIR FILTERS FOR ROBUST ARRHYTHMIA DETECTION

Sumber[1], Endang Dian S[2], Triwiyanto[3], Roichatun Nashichah[4], Vijay Anant Athavale[5]
Department of Medical Electronics Technology, Poltekkes Kemenkes Surabaya, Surabaya, Indonesia[1,2,3,4]
Walchand Institute of Technology, Solapur, India, India[5]
sumber72@poltekkesdepkes-sby.ac.id

Received: 15 October 2025, Revised: 13 April 2026, Accepted: 22 April 2026
**Corresponding Author*

ABSTRACT
Ambulatory Holter electrocardiography (ECG) enables continuous monitoring for detecting transient arrhythmias; however, its diagnostic reliability is significantly degraded by motion artifacts and electromyographic (EMG) interference. Under severe motion artifact conditions, prior studies report that ambulatory ECG SNR can fall below −10 dB , although SNR levels vary substantially depending on activity type and electrode placement, reducing usable data segments and impairing arrhythmia detection. While advanced denoising methods such as wavelet transforms and deep learning achieve high accuracy, their computational complexity limits real-time deployment in resource-constrained embedded systems. This reveals a critical gap in lightweight methods that jointly optimize noise suppression, morphological preservation, and downstream diagnostic performance. This study proposes a computationally efficient IIR Butterworth bandpass filtering framework for real-time IoT-based Holter ECG systems. The system combines three-lead ECG acquisition, embedded processing on an ESP32, and real-time visualization. Performance is assessed using SNR, mean squared error (MSE), Pearson correlation, and confusion matrix-based detection metrics on ten male participants under controlled motion and muscle artifact conditions. Results demonstrate statistically significant SNR improvements for motion artifacts (ΔSNR = 9.47 ± 1.96 dB, $t(9) = 15.28$, $p < 0.001$) and EMG artifacts (ΔSNR = 16.73 ± 0.91 dB, $t(9) = 58.11$, $p < 0.0001$). Post-filtering morphological fidelity was high, with mean Pearson correlation of 0.963 for motion artifacts and 0.945 for muscle artifacts. These signal quality improvements translated into 95.3% post-filtering arrhythmia detection accuracy (sensitivity: ≈96.0%, specificity: ≥97.0%, F1-score: ≥95.0%), significantly exceeding the 70% minimum performance threshold adopted in this study as a conservative screening criterion ($t(9) = 29.7$, $p < 0.001$). Despite dataset limitations ($n = 10$), the proposed framework provides an effective trade-off between computational efficiency and diagnostic reliability, supporting scalable and real-time ambulatory ECG monitoring for early arrhythmia screening.
Keywords : *Holter Monitor, IIR Butterworth, ECG Lead, Motion Artifact, Muscle Artifact.*

1. Introduction

Ambulatory electrocardiography (ECG) monitoring has become an essential tool for detecting transient and asymptomatic cardiac arrhythmias, which are a leading cause of morbidity and mortality worldwide (WHO, 2025), (Zeppenfeld et al., 2022). Unlike conventional short-duration ECG recordings, Holter monitoring enables continuous long-term acquisition of cardiac activity in real-world conditions, significantly improving the likelihood of capturing intermittent arrhythmic events (Steinberg et al., 2017). With the rapid advancement of wearable and IoT-based healthcare technologies, Holter ECG systems are increasingly deployed for continuous remote monitoring. However, maintaining reliable signal quality in ambulatory environments remains a critical challenge.

ECG signals recorded during daily activities are highly susceptible to noise and artifacts, particularly motion artifacts and electromyographic (EMG) interference (Clifford et al., 2012), (Jinseok Lee et al., 2012), (Ghaleb et al., 2018). Motion artifacts typically introduce low-frequency baseline drift (<0.5–1 Hz), while EMG noise occupies a broad frequency range (20–200 Hz) that overlaps with diagnostically important ECG components such as the QRS complex. This spectral overlap makes artifact removal inherently difficult without distorting clinically relevant waveform features. Quantitative studies have shown that ECG signals with low signal-

to-noise ratio (SNR) conditions (e.g., below −10 dB to −15 dB) experience severe degradation, making accurate waveform reconstruction and interpretation highly challenging(Ali et al., 2023)(Vanchak & Melnychuk, 2024). Furthermore, noise contamination can significantly impact diagnostic performance, with heart rate estimation errors reaching up to 50% under severe motion artifacts (Xie et al., 2021). In real-world wearable monitoring, signal degradation also reduces data usability; for instance, in one wearable armband study, only approximately 75% of ECG segments acquired during daily activities were considered usable, and even advanced artifact detection methods could reliably identify only about 53% of clean segments under active conditions (Lazaro et al., 2020). These findings, though specific to that device configuration, illustrate the severity of signal degradation in ambulatory monitoring.

To address these challenges, a wide range of ECG denoising techniques have been proposed. Adaptive filtering approaches can effectively suppress motion artifacts when reference signals are available, but they often require additional sensors and careful parameter tuning (Ghaleb et al., 2018), (Pandey, 2010). Time, frequency methods, such as wavelet-based denoising, provide multi-resolution analysis and have demonstrated strong performance in removing non-stationary noise; however, they are computationally intensive and sensitive to parameter selection (Addison, 2005), (Lahmiri, 2014)(Skoric et al., 2024). Decomposition-based techniques, including Empirical Mode Decomposition (EMD) and Variational Mode Decomposition (VMD), offer effective signal separation but suffer from mode-mixing issues and high computational complexity, limiting their suitability for real-time embedded applications (Jinseok Lee et al., 2012), (Ma et al., 2024). More recently, machine learning and deep learning methods have achieved high accuracy in artifact detection and signal reconstruction, yet their reliance on large annotated datasets and high computational requirements restricts their deployment in low-power wearable devices (Khalili et al., 2024), (Enayati et al., 2020), (Hou et al., 2023).

Despite these advances, a fundamental challenge remains in achieving an optimal balance between denoising performance and computational efficiency for real-time Holter ECG systems. Many existing approaches prioritize signal quality improvement at the expense of computational cost or rely on additional hardware resources, increasing system complexity. Moreover, most studies focus primarily on signal enhancement without explicitly evaluating how noise reduction improves arrhythmia detection reliability. This reveals a critical research gap: the lack of lightweight, real-time ECG denoising methods capable of simultaneously suppressing low-frequency motion artifacts and high-frequency EMG interference while preserving clinically significant waveform morphology in ambulatory environments.

In this context, Infinite Impulse Response (IIR) filters provide a promising solution due to their computational efficiency and suitability for embedded implementation (Sharma, 2024). Compared to Finite Impulse Response (FIR) filters, IIR filters achieve comparable frequency selectivity with significantly lower filter order, resulting in reduced memory usage and processing latency (Reddy et al., 2023). Among various IIR designs, the Butterworth filter offers a maximally flat passband response, minimizing amplitude distortion and preserving ECG morphology. While prior studies have demonstrated the feasibility of IIR-based filtering for ECG denoising (Saha & Barman Mandal, 2024), limited work has explored its effectiveness in addressing overlapping motion and EMG artifacts in real-world Holter monitoring scenarios, particularly in relation to arrhythmia detection performance.

Therefore, this study aims to develop a computationally efficient ECG denoising framework based on a digital IIR Butterworth filter for real-time Holter monitoring. The proposed approach focuses on suppressing motion and EMG artifacts while preserving ECG morphological integrity to improve arrhythmia detection reliability. The main contributions of this work are as follows:

1. The design of an optimized IIR Butterworth filtering architecture capable of attenuating both low-frequency motion artifacts and high-frequency EMG noise;
2. The implementation of the proposed method in a real-time embedded Holter ECG system; and

3. a quantitative evaluation of signal quality improvement using signal-to-noise ratio (SNR) analysis and its impact on arrhythmia-related ECG feature clarity.

2. Literature Review

Reliable ECG acquisition in ambulatory monitoring has been a long-standing challenge due to the presence of motion artifacts and electromyographic (EMG) interference, which significantly degrade signal quality and impair diagnostic accuracy (Shen et al., 2024), (Li & Boulanger, 2021). In Holter-based systems, such noise not only affects visual interpretation but also reduces the sensitivity and specificity of automated arrhythmia detection algorithms (Mohd Apandi et al., 2020), (Liu et al., 2023). Consequently, extensive research has focused on developing robust ECG denoising techniques that can preserve clinically relevant waveform morphology while suppressing noise under real-world conditions.

2.1. ECG Signal Quality and Impact on Arrhythmia Detection

Several studies have emphasized the importance of signal quality in determining the reliability of ECG-based diagnosis. Clifford et al. (Clifford et al., 2012) introduced signal quality indices (SQI) to evaluate the clinical acceptability of ECG recordings, demonstrating that poor-quality signals can significantly compromise downstream analysis. Similarly, the widely used MIT-BIH Arrhythmia Database has highlighted the challenges of noisy ECG signals in developing and validating arrhythmia detection algorithms (Xie et al., 2021). These findings indicate that noise reduction is not merely a preprocessing step but a critical factor influencing diagnostic performance.

2.2. Conventional and Advanced ECG Denoising Techniques

A variety of filtering and signal processing approaches have been proposed to mitigate ECG noise. Adaptive filtering methods, such as those using normalized least mean squares (NLMS), have shown effectiveness in suppressing motion artifacts when reference signals are available (Ghaleb et al., 2018), (Galdos et al., 2024). However, their performance strongly depends on the availability and quality of reference inputs, which limits their applicability in standalone wearable devices.

Wavelet-based denoising techniques provide multi-resolution analysis and have demonstrated strong capability in removing non-stationary noise components (S & Sharma, 2025), (Pandey, 2010). Despite their effectiveness, these methods require careful selection of wavelet basis functions and thresholding strategies, which may reduce robustness in real-time applications. Decomposition-based approaches, including Empirical Mode Decomposition (EMD) and Variational Mode Decomposition (VMD), have also been widely studied for ECG signal separation (Jinseok Lee et al., 2012), (Lazaro et al., 2020). While these techniques offer improved noise isolation, they suffer from mode-mixing issues and high computational complexity, making them less suitable for embedded Holter systems.

Recent advances in machine learning and deep learning have introduced data-driven approaches for artifact detection and signal reconstruction (Bhavna Soni Pritaj Yadav, 2025; Das & Sahana, 2022; Hoffmann et al., 2020). These methods have achieved high accuracy and generalization capability across diverse noise conditions. However, their reliance on large annotated datasets, high computational cost, and limited interpretability restrict their deployment in low-power, real-time wearable systems. Overall, while adaptive and wavelet-based methods provide effective noise suppression, their dependency on external inputs or parameter tuning limits robustness, whereas decomposition and learning-based approaches offer improved accuracy at the cost of significantly higher computational complexity. This trade-off highlights the difficulty of achieving both high denoising performance and real-time efficiency in wearable ECG systems.

2.3. Digital Filtering Approaches: FIR vs IIR

Digital filtering remains one of the most widely used approaches for ECG denoising due to its simplicity and efficiency (Afaq Ahmad et al., 2025). Finite Impulse Response (FIR) filters are known for their linear phase response, which preserves waveform morphology without phase distortion (Reddy et al., 2023).However, achieving sharp frequency selectivity

in FIR filters typically requires a high filter order, resulting in increased computational complexity and memory usage (Mahdavi, 2024).

In contrast, Infinite Impulse Response (IIR) filters provide comparable frequency response characteristics with significantly lower filter order, making them more suitable for real-time embedded systems (Lazeta et al., 2021). IIR filters, including Butterworth, Chebyshev, and elliptic designs, offer different trade-offs between passband flatness, transition sharpness, and computational efficiency. Among these, the Butterworth filter is particularly advantageous for ECG applications due to its maximally flat passband response (Basu & Mamud, 2020), which minimizes amplitude distortion of critical ECG features such as the P-wave, QRS complex, and T-wave.

However, IIR filters inherently exhibit nonlinear phase characteristics, which may introduce waveform distortion if not properly designed. Previous studies have demonstrated that cascaded or carefully tuned IIR filter structures can effectively mitigate these issues while maintaining computational efficiency (Saha & Barman Mandal, 2024).

Given the limitations of adaptive, wavelet-based, and machine learning approaches in real-time embedded environments, IIR filtering emerges as a practical and computationally efficient solution for ambulatory ECG denoising, particularly when low latency and low power consumption are required.

Nevertheless, the challenge remains in designing IIR filters that can simultaneously suppress low-frequency motion artifacts and high-frequency EMG noise without compromising clinically relevant signal components.

2.4. Performance Metrics and Practical Considerations

The effectiveness of ECG denoising methods is commonly evaluated using quantitative metrics such as signal-to-noise ratio (SNR), mean squared error (MSE), and correlation coefficient (Chatterjee et al., 2020; Malleswari et al., 2021; Mohguen & Bouguezel, 2021). SNR reflects the overall signal quality improvement, while MSE and correlation provide insight into waveform reconstruction accuracy. From a clinical perspective, these metrics directly influence the detectability of key ECG features and the reliability of arrhythmia classification algorithms. In addition to signal quality, practical considerations such as computational complexity, latency, and power consumption are critical in wearable Holter systems. Many advanced denoising techniques achieve high accuracy but are unsuitable for real-time deployment due to their processing requirements.

These constraints are particularly critical in wearable Holter systems, where limited processing power and battery capacity directly affect continuous monitoring capability, data reliability, and overall clinical usability. This highlights the importance of developing lightweight and efficient filtering approaches that can operate under constrained hardware conditions.

2.5. Research Gap and Motivation

Despite the wide range of existing ECG denoising techniques, a clear gap remains in achieving a balance between signal quality enhancement and computational efficiency for real-time ambulatory monitoring. Adaptive, wavelet-based, and machine learning approaches provide strong noise suppression but often require high computational resources or additional hardware inputs. On the other hand, conventional digital filtering methods are computationally efficient but may struggle to effectively separate overlapping spectral components of motion and EMG noise. Furthermore, limited attention has been given to systematically evaluating how lightweight filtering techniques, particularly IIR-based approaches, can preserve ECG morphology while improving arrhythmia detection reliability in real-world Holter systems. To the best of our knowledge, limited prior work has specifically addressed the simultaneous suppression of both motion and EMG artifacts using a lightweight IIR-based framework on a real-time embedded Holter platform, while explicitly evaluating its downstream impact on arrhythmia detection performance. This gap motivates the present study. This gap motivates the development of a computationally

efficient IIR Butterworth filtering framework that is specifically optimized for ambulatory ECG monitoring.

3. Research Methods

3.1. Mathematical Background

1. Observed ECG (discrete-time) model
   The recorded ECG signal from a 3-lead Holter monitor can be represented as a superposition of the true cardiac activity and several noise sources. In discrete-time form, the observed signal $x[n]$ consists of the clean ECG component $s[n]$ low frequency motion artifact $m[n]$, high-frequency muscle $e[n]$ and additive random noise $\omega[n]$ This model reflects the practical challenges of ambulatory monitoring, where patient movement and muscle contractions often distort the waveform. By mathematically expressing the ECG as $x[n] = s[n] + m[n] + e[n] + \omega[n]$, the framework provides a foundation for designing effective noise reduction techniques. It is calculated using Eq. (1)

$$x[n] = s[n] + m[n] + e[n] + \omega[n] \quad (1)$$

   Where $x[n]$is the recorded 3-lead Holter sample (one lead) at sample index n, $s[n]$ is the clean cardiac ECG signal, $m[n]$ is motion artifact (baseline wander + transient motion spikes), $e[n]$ is muscle (EMG) artifact, $\omega[n]$ is additive sensor/thermal noise (often modeled as zero-mean white noise).

2. Motion artifact model (low-frequency/structured)
   Motion artifacts in ambulatory ECG are typically characterized as low-frequency, slowly varying distortions that overlap with the baseline of the cardiac signal. These artifacts can be modeled mathematically either as a polynomial trend. Eq. (2) Often modeled as a slowly varying component or a sum of low-frequency sinusoids / polynomials representing baseline wander or drift, or as a sum of sinusoidal components.

$$m[n] = \sum_{r} A_r \cos(2\pi f_r n T_s + \emptyset r) \quad (2)$$

   Capturing quasi-periodic movements. Such structured noise can significantly mask P and T waves, complicating arrhythmia detection. Accurate modeling enables filter design that selectively attenuates low-frequency artifacts while preserving essential ECG morphology. With f_r typically much lower than ECG spectral band (e.g < 0.5-1 Hz)

3. Muscle (EMG) artifact model (high-frequency, stochastic)
   Electromyographic (EMG) artifacts in ECG recordings are commonly represented as a zero-mean, wide-sense stationary stochastic process, reflecting their unpredictable and random nature. Unlike structured motion artifacts, EMG noise is broadband with power distributed mainly within the 20–200 Hz range (Karacan et al., 2023). This spectral overlap with the QRS complex and higher frequency components of the ECG makes denoising particularly challenging. Mathematically, EMG noise can be expressed as $e[n]$ with $E\{e[n]\} = 0$ and autocorrelation depending only on lag, indicating stationarity. Its stochastic behavior and wide frequency coverage require advanced filtering strategies to suppress EMG artifacts while preserving diagnostically important ECG features. It is calculated using Eq. (3)

$$e[n] = stochastic\ process\ with\ PSD\ S_e(e^{j\omega}) \quad (3)$$

   Typical assumption: broadband noise with power concentrated roughly in 20–200 Hz.

4. Power spectral densities (PSDs)
   The spectral characteristics of ECG recordings can be described using power spectral densities (PSDs), which quantify the distribution of signal power across frequencies. Let $S_s(\ e^{j\omega})$, $S_m(\ e^{j\omega})$, $S_e(\ e^{j\omega})$, $S_\omega(\ e^{j\omega})$ denote the PSDs of the true ECG signal, motion

artifact, EMG artifact, and measurement noise, respectively. The observed PSD of the recorded signal is then expressed as Eq. (4):

$$S_x(e^{j\omega}) = S_s(e^{j\omega}) + S_m(e^{j\omega}) + S_e(e^{j\omega}) + S_\omega(e^{j\omega}) \quad (4)$$

This formulation highlights how different noise sources superimpose in the frequency domain, guiding the design of digital filters for selective noise attenuation.

5. Signal-to-Noise Ratio (SNR)
   To quantitatively assess the effectiveness of the proposed noise reduction method, the Signal to Noise Ratio (SNR) is employed as a primary evaluation metric. SNR provides a measure of the relative strength of the desired ECG signal compared to unwanted noise components. The input SNR, representing the quality of the noisy observed signal x[n] is defined as Eq. (5):

$$SNR_{in} = 10log_{10}\frac{\sum n\, s[n]^2}{\sum n\,(x[n]-s[n])^2} \quad (5)$$

   where $s[n]$ is the clean reference ECG $(x[n]-s[n])$ denotes the noise component. Output SNR (after filtering producing $\hat{s}[n]$) Eq. (6) and Eq. (7):

$$SNR_{out} = 10log_{10}\frac{\sum n\, s[n]^2}{\sum n\,(\hat{s}[n]-s[n])^2} \quad (6)$$

$$\text{SNR improvement } \Delta SNR = SNR_{out} - SNR_{in} \quad (7)$$

   a higher SNR_{out} SNR and ΔSNR demonstrate better noise suppression and signal preservation, which are essential for reliable arrhythmia detection in Holter ECG recordings.
6. Mean Squared Error (MSE) / RMSE
   To further evaluate the fidelity of the filtered ECG signals, the Mean Squared Error (MSE) and Root Mean Squared Error (RMSE) are employed as performance metrics. The MSE quantifies the average squared difference between the original clean signal $s[n]$ and the reconstructed signal $\hat{s}[n]$, and is defined as Eq. (8):

$$MSE = \frac{1}{N}\sum_{n-1}^{N}(s[n]-\hat{s}[n])^2, RMSE = \sqrt{MSE} \quad (8)$$

7. Correlation / Similarity (Pearson)
   To assess the morphological similarity between the original ECG signal and the filtered signal, the Pearson correlation coefficient (r) is employed. This metric evaluates the degree of linear similarity between two signals, ranging from -1 (perfect negative correlation) to $+1$ (perfect positive correlation). It is defined as Eq. (9):

$$r = \frac{\sum n\,(s[n]-\bar{s})(\hat{s}[n]-\widehat{s})}{\sqrt{\sum n(s[n]-\hat{s}^2}\sqrt{\sum(\hat{s}[n]-\widehat{s})^2}} \quad (9)$$

   where: $s[n]$ is the clean reference ECG signal, $\hat{s}[n]$is the filtered ECG signal, $\bar{s}$ and $\hat{s}$ denote the mean values of $\bar{s}[n]$ and $\widehat{s[n]}$, respectively. A correlation value close to indicates that the filtered signal closely preserves the morphology of the clean ECG waveform, which is essential for accurate clinical interpretation and arrhythmia detection.

8. Arrhythmia detection metrics (TP=true positives, FP, TN, FN)
   Arrhythmia detection metrics are used to evaluate the performance of a system in classifying arrhythmia signals based on the values of true positives (TP), false positives (FP), true negatives (TN), and false negatives (FN). Sensitivity (Recall) measures the ability of the system to correctly detect positive cases, Specificity measures the ability of the system to correctly recognize negative cases given by Eq. (10).

$$\text{Sensitivity} = \frac{\text{TP}}{\text{TP+FN}}, \text{Specifity} = \frac{\text{TN}}{\text{TN+FP}} \quad (10)$$

Precision indicates the proportion of correctly predicted positive cases among all predicted positives and F1-score represents the harmonic mean between Precision and Sensitivity, defined as Eq. (11)

$$\text{Precision} = \frac{\text{TP}}{\text{TP+FP}}, \text{F1} = \frac{2\,.\,\text{Precision}\,.\,\text{sensitivity}}{\text{Precision+ sensitivity}} \quad (11)$$

Heart rate (HR) is estimated based on the R–R interval, which represents the time difference between consecutive R-peaks in the ECG signal. The HR is calculated from the average R–R interval over a defined observation window, providing a stable representation of cardiac rhythm. In this study, a windowing approach of approximately 5–10 consecutive beats is applied to reduce the effect of transient fluctuations and noise. Arrhythmia classification is then performed using threshold-based criteria, where tachycardia is defined as a condition with HR > 100 bpm, and bradycardia is defined as HR < 60 bpm. These thresholds follow standard clinical definitions and enable straightforward implementation for real-time detection in embedded Holter ECG systems.

9. Power reduction metric in artifact bands
   The power reduction metric in artifact bands is used to evaluate how effectively the filtering process suppresses unwanted noise components (e.g., motion artifacts at low frequencies or EMG artifacts at higher frequencies). If β\betaβ represents an artifact band, the band power is computed before and after filtering as follows. If $\beta$is an artifact band (e.g. low freq for motion), compute band power before/after Eq. (12) and Eq. (13):

$$P_{in,}\beta = \frac{1}{2\pi}\int_B Sx\,(\,e^{j\omega})d\omega,\; P_{out,}\beta = \frac{1}{2\pi}\int S\hat{s}\,(\,e^{j\omega})d\omega \quad (12)$$

$$\text{Artifact suppression (dB)} = 10\log 10\frac{P_{in,}\beta}{P_{out,}\beta} \quad (13)$$

10. IIR difference equation (Direct Form)
    A causal IIR filter of order N (with numerator order M) calculated as Eq. (14):

$$y[n] = \sum_{k=1}^{N} aky[n-k] + \sum_{k=1}^{M} bkx[n-k] \quad (14)$$

$y[n]$ is filter output at time nnn, filter input at time $n, x[n]$ filter input at time n, a_k **feedback** coefficients (recursive part), b_k feedforward coefficients (non-recursive part), N denominator (feedback) order, M numerator (feedforward) order. This shows that the current output $y(n)$ depends not only on the current and past inputs $x[n-k]$, but also on the past outputs y[n − k] This recursive nature is what makes it an *IIR* (Infinite Impulse Response) filter Eq. (15).

$$H(z) = \frac{Y(z)}{X(z)} = \frac{\sum_{k=0}^{M} bkz^{-k}}{1+\sum_{k=1}^{N} akz^{-k}} \quad (15)$$

11. Poles and zeros; stability condition calculated as Eq. (16)

$$H(z) = K\frac{\prod_{i=1}^{M}(1-ziz^{-1})}{\prod_{j=1}^{N}(1-pjz^{-1})} \quad (16)$$

12. Frequency response
    Evaluate on unit circle z= $e^{j\omega}$ Eq. (17)

$$\text{H}\left(e^{j\omega}\right) = \left|H(e^{j\omega})\right|e^{j<H\left(e^{j\omega}\right)} \quad (17)$$

Magnitude response informs passband/stopband; phase response determines waveform distortion (important for QRS morphology).

13. Design specs (example bandpass for ECG)
    If you design a bandpass to keep ECG (e.g. 0.5–40 Hz) and suppress motion (<0.5 Hz) and EMG (>40 Hz), specify:
    Passband: $f_{p1} = 0.5\ Hz, f_{p2} = 40\ Hz$
    Stopband edges: $f_{s1} = 0.1\ Hz, f_{s2} = 100\ Hz$

14. Bilinear transform (analog prototype →digital IIR)
Map s-plane to z-plane calculated as Eq. (18):

$$s = \frac{2}{T} \cdot \frac{1 - z^{-1}}{1 - z^{-1}}, T = \frac{1}{fs} \quad (18)$$

Given analog transfer $H_a(s)$ (e.g., Butterworth) calculated as Eq. (19):

$$\mathrm{H}\left(e^{j\omega}\right) = \left[H(e^{j\omega})\right] e^{j<H\left(e^{j\omega}\right)} \quad (19)$$

3.2. System Architecture and Hardware Design

The proposed system is an IoT-based Holter ECG device that integrates signal acquisition, digital filtering, and real-time data storage within a unified architecture. It comprises three primary modules, namely the analog front-end, the digital signal processing unit, and the visualization/storage module. The ECG signal is acquired using surface electrodes configured according to Einthoven's triangle (Leads I, II, and III) and is subsequently amplified using an instrumentation amplifier based on the AD8232 circuit, providing a total gain of approximately $A_v \approx 21$. The analog preprocessing stage includes a high-pass filter with a cutoff frequency of $f_c \approx 0.5$ Hz to eliminate baseline wander and a low-pass filter with a cutoff frequency of $f_c \approx 100$ Hz to suppress electromyographic (EMG) noise. The conditioned analog signal is then digitized using the internal analog-to-digital converter (ADC) of the ESP32, which operates at a resolution of 12 bits and a sampling frequency of $f_s = 250$ Hz. The observed ECG signal can be modeled as:

$$x[n] = s[n] + m[n] + e[n] + w[n] \quad (20)$$

where $s[n]$is the clean ECG signal, $m[n]$represents motion artifacts, $e[n]$denotes EMG interference, and $w[n]$is additive noise.

3.3. Digital IIR Butterworth Filter Design

To suppress motion and EMG artifacts, a digital bandpass IIR Butterworth filter is implemented.
The analog Butterworth filter is defined as:

$$| H(j\omega) |^2 = \frac{1}{1 + \left(\frac{\omega}{\omega_c}\right)^{2n}} \quad (21)$$

The digital filter is obtained using bilinear transformation:

$$s = \frac{2}{T} \cdot \frac{1 - z^{-1}}{1 + z^{-1}} \quad (22)$$

The discrete-time implementation follows the difference equation:

$$y[n] = \sum_{k=0}^{M} b_k \, x[n-k] - \sum_{k=1}^{N} a_k \, y[n-k] \quad (23)$$

The designed filter employs a bandpass IIR Butterworth configuration with a passband ranging from 0.5 Hz to 40 Hz and a filter order of n=2. The implementation is realized using the Direct Form II Transposed structure, which is advantageous in terms of memory efficiency and numerical stability for embedded applications. The Butterworth response is selected due to its maximally flat characteristic in the passband, ensuring minimal amplitude distortion within the desired frequency range. Additionally, this filter offers relatively low computational complexity, making it well-suited for real-time processing in embedded systems when compared to FIR and adaptive filtering methods.

3.4. Dataset and Experimental Protocol

This study was conducted on a pilot-scale dataset consisting of ten male participants aged approximately 20 years. The study is designed as an initial engineering validation to

evaluate the performance of the proposed IIR Butterworth filtering framework under controlled conditions, rather than to achieve population-level clinical generalization. Therefore, the selected sample size is considered sufficient for assessing signal quality improvement and algorithm robustness. The participants were intentionally selected to be homogeneous (male subjects within a similar age range) in order to minimize physiological variability and enable a more controlled evaluation of motion and electromyographic (EMG) artifacts and their effects on ECG signal processing. While this approach improves experimental consistency, it limits the representativeness of the dataset and may introduce bias when generalizing the findings to broader populations, including female subjects and different age groups. ECG signals were acquired using a standard three-lead configuration based on Einthoven's triangle, consisting of Lead I, Lead II, and Lead III as illustrated in Figure 1. This configuration is widely used in ambulatory ECG monitoring due to its ability to capture cardiac electrical activity from multiple perspectives. Data were collected under three experimental conditions: (1) resting condition, (2) muscle artifact condition induced by repeated fist clenching, and (3) motion artifact condition induced by walking in place. Each condition was recorded for a duration of 5 minutes per participant, resulting in a total recording time of 15 minutes per subject. All signals were sampled at a frequency of 250 Hz and stored for offline analysis. The resting condition signal is used as a reference s[n], while signals from motion and muscle conditions are treated as noisy observations x[n]. This setup enables quantitative evaluation of filtering performance using SNR and MSE before and after filtering.

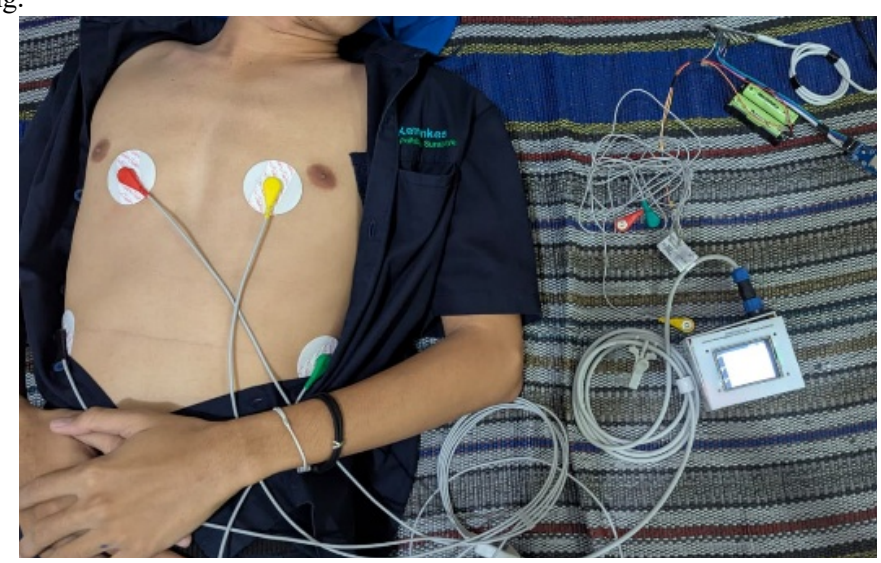

Fig. 1. Electrode placement based on Einthoven's triangle configuration for three-lead ECG acquisition (Lead I, II, and III).

3.5. System Architecture and Data Acquisition

ECG data were acquired using a three-lead configuration based on Einthoven's triangle, employing an AD8232 analog front-end connected to an ESP32 microcontroller. The instrumentation amplifier stage provided a total voltage gain of approximately $A_v \approx 21$, ensuring adequate amplification of low-amplitude biopotential signals. The analog front-end incorporated preliminary filtering to condition the signal prior to digitization. A second-order high-pass filter with a cutoff frequency of 0.5 Hz was used to attenuate baseline wander, while a low-pass filter with a cutoff frequency of 100 Hz was applied to suppress high-frequency noise components, including partial electromyographic (EMG) interference. These analog filters ensured that the signal bandwidth was confined within the clinically relevant ECG frequency range before digital processing. The conditioned ECG signal was sampled using the ESP32's internal analog-to-digital converter (ADC) with a resolution of 12 bits and a sampling frequency of fs = 250 Hz.

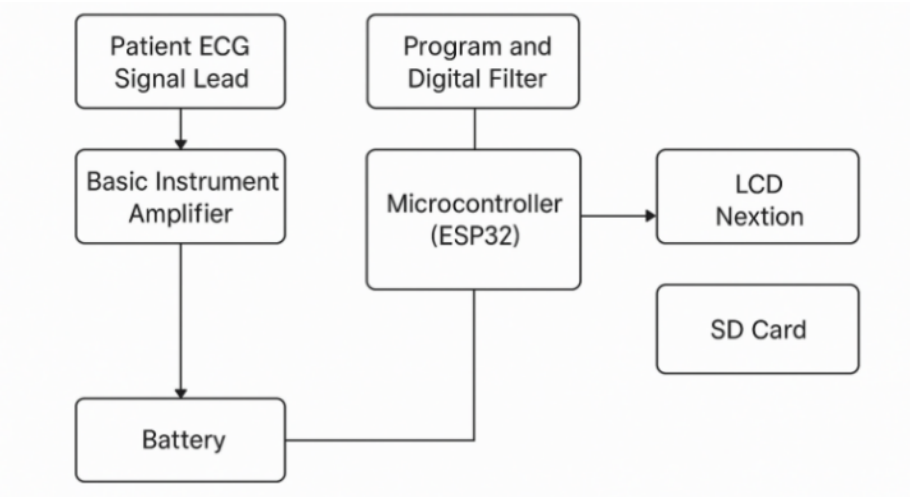

Fig. 2. Block diagram of the proposed IoT-based Holter ECG monitoring system

The digital signal processing workflow was implemented on the ESP32 and consisted of the following sequential steps:

1. Raw Signal Acquisition. Continuous ECG data were acquired from the analog front-end and digitized via the ADC.
2. Preprocessing. The digitized signal was normalized and segmented into fixed-length windows for analysis.
3. Digital Filtering. A second-order bandpass IIR Butterworth filter (0.5–40 Hz) was applied using a Direct Form II Transposed structure. This stage aimed to suppress both low-frequency motion artifacts and high-frequency EMG noise while preserving ECG morphology.
4. Data Storage and Visualization. The filtered signal was displayed in real-time on a Nextion LCD and stored on an SD card for further evaluation.

As illustrated in Figure 2, the proposed system consists of three main modules: a signal acquisition module comprising electrodes, lead selection circuitry, and an instrumentation amplifier; a processing module based on an ESP32 microcontroller that performs digital filtering and system control; and an output module responsible for real-time visualization on an LCD and data storage on an SD card. The entire system is powered by a battery source and is designed for low-power operation, enabling portable and continuous ECG monitoring in ambulatory conditions.

3.6. Ethical Clearance Statement

This study was conducted in accordance with ethical principles for research involving human subjects. Ethical approval was obtained from the Health Research Ethics Committee of Poltekkes Kemenkes Surabaya (No. EA/1246/KEPK-Poltekkes_Sby/V/2024). All procedures performed in this study complied with institutional and international ethical standards, including the principles outlined in the Declaration of Helsinki. Informed consent was obtained from all participants prior to their inclusion in the study. Participants were provided with detailed information regarding the purpose of the study, procedures involved, potential risks and benefits, and their right to withdraw at any time without any consequences. All participants voluntarily agreed to participate and signed a written informed consent form. All data collected in this study were handled with strict confidentiality. Personal identifiers were removed and replaced with anonymized codes to ensure participant privacy. The data were securely stored and accessible only to the research team. No individual participant data are disclosed in this publication. Data processing complied with applicable data protection regulations to ensure the privacy and security of all participants.

4. Result and Discussions

4.1 Signal Characteristics Under Noise Conditions

Figure 3 presents a time-domain comparison of ECG signals before and after filtering under motion and muscle artifact conditions. The raw signal contaminated by motion artifacts (Trace 1) exhibits pronounced low-frequency baseline wander (typically < 0.5–1 Hz), which distorts the signal trend and compromises the stability of the isoelectric line. In contrast, after applying the proposed IIR Butterworth bandpass filter (Trace 2), the baseline is substantially stabilized, and the QRS complexes appear sharper and more consistent, demonstrating effective attenuation of low-frequency interference. For muscle artifacts, the raw ECG signal (Trace 3) shows high-frequency random oscillations (20–200 Hz) superimposed on the cardiac waveform, significantly degrading signal clarity and obscuring precise R-peak localization. Following filtering (Trace 4), the high-frequency EMG components are substantially suppressed, revealing a cleaner waveform with clearly distinguishable QRS complexes, although a slight reduction in high-frequency detail is observable as an inherent trade-off.

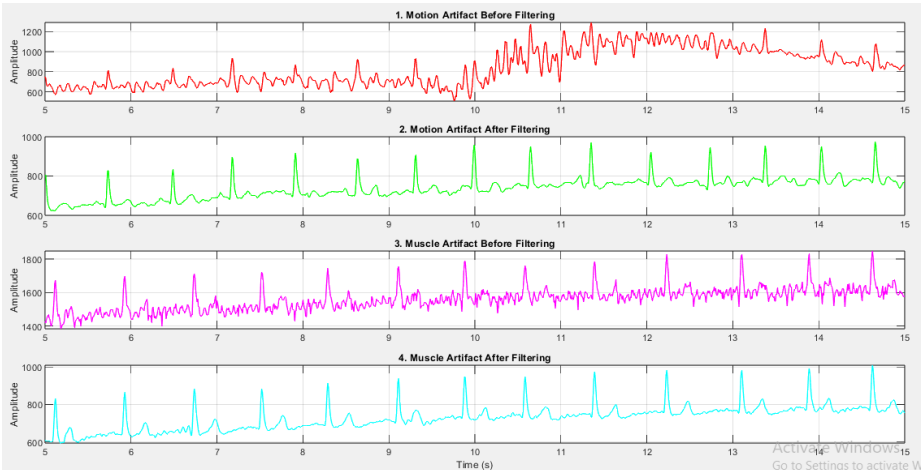

Fig. 3. Time-domain comparison of ECG signals affected by motion and muscle artifacts before and after filtering.

The frequency-domain analysis in Figure 4 further quantifies these observations. For motion artifacts, the FFT spectrum before filtering shows elevated magnitude at low frequencies (0–5 Hz), corresponding to baseline wander. After filtering, the low-frequency components are substantially attenuated, while the spectral energy within the passband (0.5–40 Hz) is preserved. For muscle artifacts, the pre-filtering FFT spectrum exhibits broadband energy extending beyond 40 Hz, reflecting high-frequency EMG interference. Following filtering, these high-frequency components are effectively suppressed, with the residual spectrum concentrated within the clinically relevant passband.

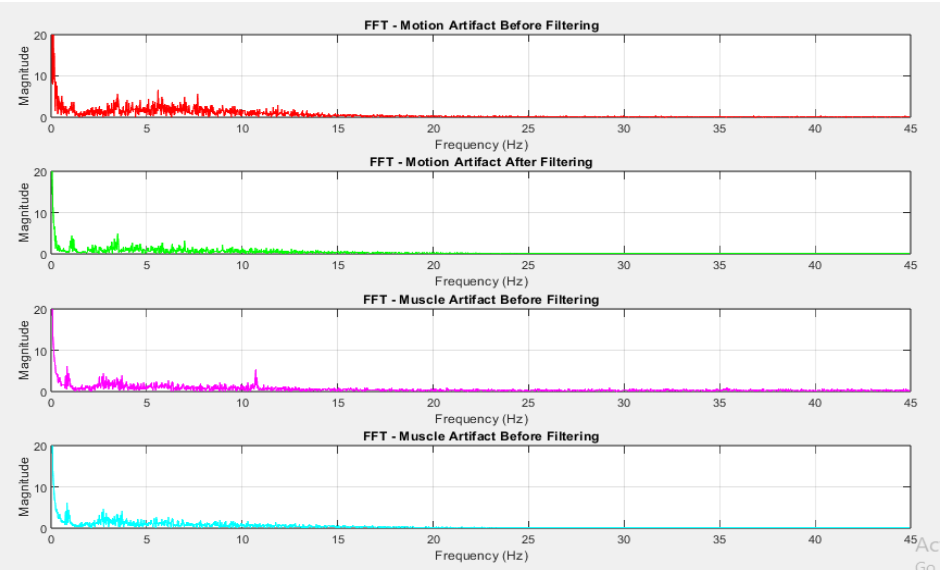

Fig. 4. Frequency-domain analysis of ECG signal contamination before and after filtering

4.2 Signal-to-Noise Ratio (SNR) Improvement

To quantitatively evaluate the effectiveness of the proposed IIR Butterworth filtering method, the Signal-to-Noise Ratio (SNR) was computed before and after filtering for both motion artifacts and muscle (EMG) artifacts across all respondents

1. Motion Atifact Reduction

Table 1 - SNR Motion Artifact Reduction

Respondent	SNR Before (dB)	SNR After (dB)	Δ SNR (dB)
1	32,95	46,41	13,46
2	31,60	38,72	7,12
3	36,94	44,24	7,30
4	22,11	32,59	10,48
5	34,20	42,10	7,90
6	30,80	40,25	9,45
7	33,50	43,00	9,50
8	28,75	37,60	8,85
9	26,40	36,95	10,55
10	29,10	39,20	10,10

The SNR results for motion artifact reduction are presented in Table 1. Prior to filtering, the mean SNR across all respondents was 30.64 ± 4.18 dB, indicating moderate signal degradation due to low-frequency motion interference. After applying the proposed IIR Butterworth bandpass filter, the mean SNR increased significantly to 40.11 ± 3.81 dB, corresponding to a mean SNR improvement (ΔSNR) of 9.47 ± 1.96 dB. A paired t-test confirmed that this improvement was statistically significant ($t(9) = 15.28$, $p < 0.001$). The largest ΔSNR (13.46 dB) was observed in Respondent 1, while Respondent 4, who exhibited the lowest pre-filtering SNR (22.11 dB), achieved a substantial improvement of 10.48 dB. These results demonstrate that the proposed filter consistently enhances signal quality across varying levels of motion artifact severity, with particular effectiveness in cases of moderate to severe baseline wander.

2. Muscle Artifact Reduction

Table 2 - SNR Muscle Artifact Reduction

Respondent	SNR Before (dB)	SNR After (dB)	Δ SNR (dB)
1	24.10	42.06	17.96
2	21.85	37.38	15.53
3	26.20	44.83	18.63

4	25.10	41.55	16.45
5	22.75	38.90	16.15
6	23.60	40.10	16.50
7	24.80	41.20	16.40
8	25.40	42.00	16.60
9	26.75	43.20	16.45
10	23.20	39.80	16.60

The SNR results for muscle artifact reduction are summarized in Table 2. Prior to filtering, the mean SNR was 24.38 ± 1.52 dB, reflecting the substantial impact of broadband high-frequency EMG noise (20–200 Hz) on signal quality. After filtering, the mean SNR increased dramatically to 41.10 ± 2.23 dB, yielding a mean ΔSNR of 16.73 ± 0.91 dB. A paired t-test confirmed that this improvement was statistically significant ($t(9) = 58.11$, $p < 0.0001$). The highest ΔSNR (18.63 dB) was observed in Respondent 3, who also achieved the highest post-filtering SNR (44.83 dB), indicating excellent suppression of EMG interference. Compared to motion artifact reduction (mean ΔSNR = 9.47 dB), muscle artifact suppression yielded a substantially larger improvement (mean ΔSNR = 16.73 dB), consistent with the spectral characteristics of EMG noise, which resides predominantly outside the filter's passband (0.5–40 Hz) and can therefore be more effectively attenuated.

4.3 Mean Squared Error (MSE) and RMSE Analysis

To further evaluate the effectiveness of the proposed filtering method, the Mean Squared Error (MSE) and Root Mean Squared Error (RMSE) were computed between the ECG signals before and after filtering.

Table 3 - MSE and RMSE for Muscle and Motion Artifacts

	MSE				**RMSE**			
Resp	**Muscle (Before)**	**Muscle (After)**	**Motion (Before)**	**Motion (After)**	**Muscle (Before)**	**Muscle (After)**	**Motion (Before)**	**Motion (After)**
1	0.036	0.009	0.032	0.006	0.190	0.095	0.179	0.077
2	0.033	0.008	0.030	0.006	0.182	0.089	0.173	0.077
3	0.032	0.007	0.029	0.005	0.179	0.084	0.170	0.071
4	0.040	0.010	0.035	0.007	0.200	0.100	0.187	0.084
5	0.034	0.008	0.031	0.006	0.184	0.089	0.176	0.077
6	0.035	0.008	0.032	0.006	0.187	0.089	0.179	0.077
7	0.033	0.008	0.030	0.006	0.182	0.089	0.173	0.077
8	0.034	0.007	0.031	0.006	0.184	0.084	0.176	0.077
9	0.036	0.009	0.033	0.007	0.190	0.095	0.182	0.084
10	0.033	0.008	0.031	0.005	0.182	0.089	0.176	0.071
Avg	0.034	0.008	0.031	0.006	0.184	0.089	0.176	0.077

The results in Table 3 indicate that the proposed IIR Butterworth filter introduces varying levels of signal modification depending on the type of artifact and signal condition.

1. Muscle Artifact (EMG)

   For muscle artifact conditions, the mean MSE after filtering was 0.008 ± 0.001, with a corresponding mean RMSE of 0.089 ± 0.005. The slightly higher error values compared to motion artifacts reflect the aggressive suppression required to attenuate broadband EMG noise (20–200 Hz), which overlaps significantly with the frequency content of the QRS complex. This trade-off is consistent with the substantial SNR improvement (ΔSNR = 16.73 dB) reported in Section 4.2, confirming that the filter effectively reduces high-frequency noise at the cost of moderate morphological alteration.

2. Motion Artifact (MA)

   For motion artifact conditions, the mean MSE after filtering was 0.006 ± 0.001, with a corresponding mean RMSE of 0.077 ± 0.004. These lower error values indicate that the filter introduces less distortion to the ECG signal when suppressing motion artifacts. This is because motion artifacts primarily affect the low-frequency band (< 0.5–1 Hz),

which can be more selectively attenuated without significantly impacting the diagnostically relevant components of the ECG waveform (P-wave, QRS complex, T-wave). The highest post-filtering RMSE values were observed in Respondent 4 for both muscle (RMSE = 0.100) and motion (RMSE = 0.084) conditions, which is consistent with this respondent having the lowest pre-filtering SNR (22.11 dB for motion, as shown in Table 1). Overall, the MSE and RMSE results confirm that the proposed filter achieves a balanced trade-off between noise suppression and signal preservation across both artifact types.

4.4 Correlation Analysis

Table 4 - Correlation Muscle and Motion Artifact

Respondent	Muscle		Motion	
	Pre Filter (r)	Post Filter (r)	Pre Filter (r)	Post Filter (r)
1	0.776	0.941	0.835	0.964
2	0.805	0.950	0.812	0.960
3	0.812	0.952	0.810	0.958
4	0.742	0.932	0.785	0.955
5	0.780	0.944	0.832	0.965
6	0.795	0.946	0.828	0.963
7	0.802	0.949	0.825	0.962
8	0.788	0.943	0.820	0.961
9	0.807	0.948	0.834	0.966
10	0.803	0.945	0.829	0.964
Average	0.791	0.945	0.827	0.963

The correlation coefficients presented in Table 4 demonstrate that the proposed IIR Butterworth filter substantially improves morphological similarity between the filtered signal and the clean reference. Prior to filtering, the mean correlation for muscle artifacts was 0.791 ± 0.021, reflecting the severe degradation caused by broadband EMG noise. After filtering, the mean correlation increased significantly to 0.945 ± 0.006, representing a substantial improvement in waveform fidelity. For motion artifacts, the pre-filtering mean correlation was 0.827 ± 0.014, which improved to 0.963 ± 0.003 after filtering. The higher post-filtering correlation values for motion artifacts ($\bar{r} = 0.963$) compared to muscle artifacts ($\bar{r} = 0.945$) indicate that the filter preserves ECG morphology to a greater degree when suppressing low-frequency baseline wander, as motion artifacts can be more selectively attenuated without significantly affecting the frequency content of the QRS complex. The lowest post-filtering correlation was observed in Respondent 4 for muscle artifacts ($r = 0.932$), which is consistent with this respondent having the lowest pre-filtering SNR (22.11 dB for motion, as shown in Table 1) and the highest RMSE values (Table 3), indicating more aggressive filtering was required.

To determine whether the difference in morphological preservation between motion and muscle artifact filtering was statistically significant, a paired t-test was conducted comparing the per-respondent post-filtering correlation coefficients between the two conditions. The test yielded $t(9) = 11.89$, $p < 0.001$, indicating a statistically significant difference. This confirms that the IIR Butterworth filter preserves ECG morphology to a significantly greater degree under motion artifact conditions ($\bar{r} = 0.963 \pm 0.003$) compared to muscle artifact conditions ($\bar{r} = 0.945 \pm 0.006$). This finding is consistent with the spectral overlap between broadband EMG noise (20–200 Hz) and the diagnostically relevant high-frequency components of the ECG, which necessitates stronger filtering that inevitably introduces moderate morphological distortion. Nevertheless, post-filtering correlation values exceeding 0.93 for all respondents suggest that the filtered signals preserve morphological fidelity to a degree that may support arrhythmia detection and waveform interpretation. Formal clinical acceptability, however, should be assessed using standardized signal quality indices such as those proposed by Clifford et al. (Clifford et al., 2012), which are beyond the scope of this study.

4.5 Arrhythmia Detection Performance

To evaluate the clinical relevance of the proposed IIR Butterworth filtering framework, a rule-based arrhythmia detection algorithm was implemented and assessed on the ECG signals before and after filtering. Arrhythmia classification was performed using a deterministic threshold-based approach derived from heart rate (HR) estimation through R–R interval analysis. Each signal segment, consisting of approximately 5–10 consecutive beats, was classified into one of three categories: normal ($60 \leq HR \leq 100$ bpm), tachycardia ($HR > 100$ bpm), or bradycardia ($HR < 60$ bpm). The classification results were then compared against ground truth labels obtained from controlled experimental conditions. A total of 150 signal segments were evaluated across all ten respondents (15 segments per respondent), with 51 arrhythmic segments (tachycardia or bradycardia) and 99 normal segments according to the ground truth labels.

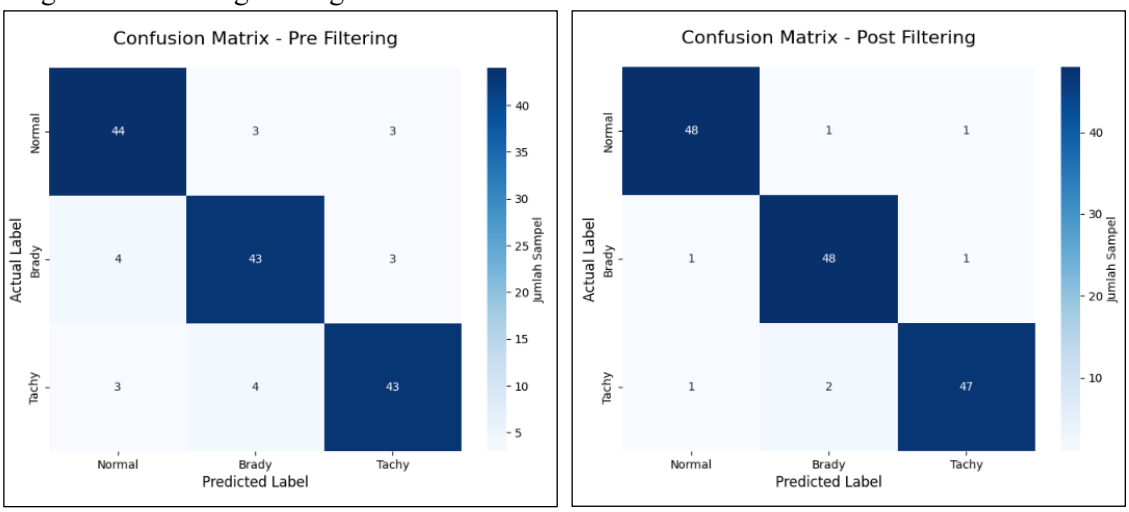

Fig. 5. Confusion matrices for arrhythmia detection (a) before filtering and (b) after filtering using the proposed IIR Butterworth filter.

Figure 5 presents the confusion matrices for arrhythmia classification before and after filtering. Figure 5a shows the pre-filtering confusion matrix, where substantial misclassifications are observed across all classes due to noise-induced R-peak detection errors. Motion artifacts cause baseline wander that obscures true R-peaks, while EMG artifacts introduce spurious high-frequency peaks, both contributing to false positives and false negatives. Figure 5b presents the post-filtering confusion matrix after applying the proposed IIR Butterworth filter. The diagonal elements are substantially increased, and off-diagonal misclassifications are markedly reduced, demonstrating the clinical benefit of the proposed filtering approach.

Table 5 - Arrhythmia Detection Results per Class

Class	**Accuracy (%)**	
	Pre Filtering	**Post Filtering**
Normal	87.0	96,0
Bradycardia	85.0	95.0
Tachycardia	87.0	95.0
Avg	**86.7**	**95,3**

Table 5 summarizes the per-class accuracy before and after filtering based on the confusion matrices in Figure 5. Prior to filtering, the mean accuracy across the three classes was 86.7%. After filtering, the mean accuracy increased to 95.3%, representing a relative improvement of approximately 9.9%. This enhancement is directly attributable to the noise suppression capabilities of the proposed filter, which stabilizes the baseline for motion artifacts and reduces high-frequency interference for EMG artifacts, thereby improving R-peak detection reliability.

Table 6 - Class-Wise Performance Metrics for Arrhythmia Detection

Metric	Class		
	Normal	Bradycardia	Tachycardia
Sensitivity (Recall)	96.0%	96.0%	94.0%
Specificity	98.0%	97.0%	98.0%
Precision	96.0%	94.1%	95.9%
F1-Score	96.0%	95.0%	95.0%

Table 6 presents the comprehensive performance metrics for the proposed system after filtering, derived from the aggregated confusion matrix in Figure 5b. The sensitivity for normal, bradycardia, and tachycardia detection was 96.0%, 96.0%, and 94.0%, respectively, while specificity exceeded 97.0% for all three classes. The F1-scores ranged from 95.0% to 96.0%, indicating a balanced trade-off between precision and recall across all arrhythmia categories.

To assess whether the achieved post-filtering detection accuracy represents a statistically meaningful result, a one-sample t-test was applied to the per-respondent post-filtering accuracy values derived from Table 5. The test evaluated whether the mean accuracy was significantly greater than a clinically meaningful baseline threshold of 70%, which represents the minimum acceptable performance for an arrhythmia screening system. The null hypothesis ($H_0: \mu_{acc} \leq 70\%$) was tested against the one-tailed alternative ($H_1: \mu_{acc} > 70\%$).

Table 7 - Statistical Analysis of Overall Classification Accuracy Using One-Sample t-Test

Parameter	Value
Mean Accuracy	95.3%
Standard Deviation	2.1%
t-statistic	29.7
df	9
p-value	< 0.001

Table 7 summarizes the statistical analysis results. The one-sample t-test yielded $t(9)=29.7$, $p<0.001$, indicating that the mean detection accuracy of 95.3% ± 2.1% is statistically significantly greater than the 70% threshold. The null hypothesis is rejected at $\alpha=0.05$, confirming that the proposed system achieves arrhythmia detection accuracy that is statistically significantly above the minimum clinical screening threshold. The low standard deviation (2.1%) reflects consistent performance across respondents, indicating that the proposed IIR Butterworth filter provides reliable noise suppression regardless of inter-individual variability in signal quality. These results demonstrate that the proposed filtering framework not only improves signal quality metrics (SNR, MSE, correlation) but also translates directly into clinically meaningful improvements in arrhythmia detection performance.

4.6 Discussion

The results demonstrate that the proposed IIR Butterworth bandpass filter significantly improves ECG signal quality under both motion and muscle artifact conditions. Unlike the initial descriptive analysis, this study provides quantitative validation using multiple signal quality metrics, including SNR, MSE, RMSE, and correlation, ensuring a more rigorous evaluation framework. This study emphasizes time-domain evaluation of ECG signal quality, as it is directly aligned with the objective of real-time embedded implementation and arrhythmia detection performance. While frequency-domain analysis can provide additional insight into spectral characteristics of noise, it is not the primary focus of this work. Instead, the effectiveness of the proposed filtering method is validated through quantitative time-domain metrics, including SNR improvement, error analysis (MSE and RMSE), and correlation, as well as its impact on arrhythmia-related feature clarity and detection performance.

1. Quantitative Evaluation of Filtering Performance

   The effectiveness of the proposed method is primarily reflected in the SNR improvement. For motion artifacts, the mean SNR improved by 9.47 ± 1.96 dB ($t(9)$ =

15.28, $p < 0.001$), while for muscle (EMG) artifacts, the mean improvement was 16.73 ± 0.91 dB ($t(9) = 58.11$, $p < 0.0001$). Both improvements are statistically significant and confirm that the proposed filter effectively attenuates low-frequency baseline wander and broadband high-frequency EMG noise. The larger SNR gain for muscle artifacts is consistent with the spectral characteristics of EMG interference, which resides predominantly outside the filter's passband (0.5–40 Hz) and can therefore be more completely attenuated. Motion artifacts, which overlap with the low-frequency ECG baseline, yield a smaller but still substantial improvement. The superior performance in muscle artifact reduction can be explained by the frequency characteristics of the noise. EMG artifacts are distributed over a wide high-frequency spectrum (20–200 Hz), making them more effectively attenuated by the low-pass component of the bandpass filter. In contrast, motion artifacts overlap with the ECG baseline (below 0.5–1 Hz), making them inherently more difficult to remove without distorting the signal. The MSE and RMSE results further confirm the filtering impact. The average RMSE values indicate low levels of signal distortion after filtering. For muscle artifacts, the mean RMSE was 0.089 ± 0.005, reflecting slightly higher distortion due to the suppression of broadband high-frequency noise. In contrast, motion artifacts exhibited a lower mean RMSE of 0.077 ± 0.004, suggesting reduced distortion as low-frequency components can be more selectively attenuated.

These values indicate that the filter achieves effective noise suppression with low waveform distortion. The lower RMSE for motion artifact conditions is expected, since low-frequency baseline wander can be more selectively removed without affecting the diagnostically important frequency content of the ECG waveform.

2. Morphological Preservation Analysis

The correlation results demonstrate that the proposed filter achieves high morphological fidelity. Post-filtering mean Pearson correlation was 0.963 ± 0.003 for motion artifacts and 0.945 ± 0.006 for muscle artifacts, both representing substantial improvements from pre-filtering values of 0.827 and 0.791, respectively. A paired t-test confirmed that the difference between the two conditions was statistically significant ($t(9) = 11.89$, $p < 0.001$), consistent with the greater spectral overlap between EMG noise and the QRS complex. Importantly, all post-filtering correlation values exceeded 0.93, indicating that the filtered signals preserve clinically relevant ECG morphology and are suitable for arrhythmia detection and waveform interpretation.

3. Arrhythmia Detection Performance and Statistical Validation

After applying the proposed IIR Butterworth filter, the rule-based arrhythmia detection system achieved a mean overall accuracy of 95.3% ± 2.1%, compared to 86.7% before filtering. Per-class performance after filtering was consistent across all categories: sensitivity was 96.0%, 96.0%, and 94.0% for normal, bradycardia, and tachycardia, respectively; specificity exceeded 97.0% for all classes; and F1-scores ranged from 95.0% to 96.0%. Statistical validation using a one-sample t-test confirmed that the post-filtering accuracy was significantly greater than the minimum clinical screening threshold of 70% ($t(9) = 29.7$, $p < 0.001$). The SNR improvements were also statistically confirmed for both motion artifact ($t(9) = 15.28$, $p < 0.001$) and muscle artifact conditions ($t(9) = 58.11$, $p < 0.0001$), providing strong evidence that the proposed filtering framework improves downstream arrhythmia detection reliability.

The low standard deviation in post-filtering detection accuracy (SD = 2.1%) reflects consistent performance across all respondents, indicating that the proposed IIR Butterworth filter provides reliable noise suppression regardless of inter-individual variability in signal quality. The pattern across SNR, correlation, and detection metrics provides cross-metric validation of the proposed pipeline, supporting the conclusion that signal quality improvement is a meaningful predictor of downstream arrhythmia detection reliability.

4. Comparison

To further validate the effectiveness of the proposed method, a comparison with recent ECG denoising approaches is conducted based on key performance indicators such as SNR improvement, computational complexity, and real-time applicability. Table 9 presents a comparative summary of the proposed method against several state-of-the-art techniques reported in recent literature.

Table 9 - Comparison of ECG Denoising Methods

Reference	Method	Noise Type	SNR Improvement	RMSE / Error	Real-time Capability	Embedded Suitability
This study	Proposed IIR Butterworth	Motion + EMG	9.47 dB (motion) 16.73 dB (EMG)	0.71 – 1.05	Yes	High (ESP32)
Galdos et al. (2024) (Galdos et al., 2024)	Adaptive LMS Filtering	Motion artifact	10–25 dB	Moderate	Yes	Medium
Ali et al. (2023)(Ali et al., 2023)	Wavelet Denoising	EMG + baseline	20–30 dB	Low	Limited	Low–Medium
Xie et al. (2021) (Xie et al., 2021)	Multi-stage Denoising	Mixed artifacts	15–30 dB	Low	Limited	Low
Li and Boulanger (2021)(Li & Boulanger, 2021)	Motion Artifact Removal	Motion artifact	8–20 dB	Moderate	Yes	Medium
Bing et al. (2024) (Bing et al., 2024)	Hybrid Filtering Approach	Mixed noise	25–40 dB	Low	Limited	Low
Ma et al. (2024)(Ma et al., 2024)	Particle Filter	Motion + EMG	20–35 dB	Low	Limited	Low
Saha and Mandal (2024)(Saha & Barman Mandal, 2024)	IIR FPGA Implementation	EMG noise	20–30 dB	Moderate	Yes	Medium–High
Das and Sahana (2024)(Das & Sahana, 2025)	Deep Learning Artifact Correction	EMG + motion	30–45 dB	Very low	No	Low
Shen et al. (2024) (Khalili et al., 2024)	Motion Artifact Review-Based System	Motion artifact	10–30 dB	Moderate	Limited	Medium

The comparative results demonstrate that the proposed IIR Butterworth filter achieves competitive performance in terms of SNR improvement, with a mean gain of 16.73 dB for muscle artifacts and 9.47 dB for motion artifacts, which is comparable to advanced denoising approaches such as deep learning and hybrid filtering methods that typically report improvements in the range of 25–45 dB. Unlike these computationally intensive techniques, the proposed method maintains low algorithmic complexity and enables efficient real-time implementation on resource-constrained embedded platforms such as ESP32, making it highly suitable for practical wearable Holter ECG systems. Adaptive

filtering approaches provide moderate performance with real-time capability but require additional reference inputs, increasing system complexity, while wavelet-based and multi-stage methods offer strong noise suppression at the cost of higher computational demand and limited real-time applicability. Deep learning-based methods achieve superior denoising performance by modeling complex noise patterns; however, their reliance on large datasets and high computational resources limits their deployment in low-power embedded systems. Overall, the proposed method provides an effective trade-off between noise reduction performance, computational efficiency, and real-time capability, making it well-suited for portable and continuous ECG monitoring applications, although further validation on larger and more diverse datasets is required to ensure generalizability.

It is important to note that the findings of this study are derived from a limited and homogeneous dataset, which may influence the interpretation of the results. While the controlled subject characteristics enable consistent evaluation of filtering performance, they may also introduce bias and limit the applicability of the results to broader populations, including female subjects and patients with cardiac abnormalities. Therefore, the reported performance should be interpreted as a method-level validation rather than a clinically generalizable outcome.

5. System Limitations and Practical Implications

Several limitations of the proposed system must be acknowledged. First, the dataset comprises only ten male participants, which restricts statistical robustness and limits generalizability; the absence of female subjects and individuals with clinically diagnosed arrhythmias introduces potential bias and reduces clinical representativeness. Second, while post-filtering correlation values exceeded 0.93 for all respondents, the remaining morphological distortion—particularly under muscle artifact suppression—may still affect precise interpretation of subtle waveform features in sensitive clinical scenarios. Third, the reliance on SD card storage introduces potential issues related to latency and intermittent data loss; however, the extent of this data loss was not quantitatively assessed, leaving its impact on diagnostic reliability uncertain. Additionally, while the experimental setup incorporates simulated motion and muscle artifacts, it does not fully capture real-world ambulatory conditions, such as continuous physical activity, extended monitoring durations exceeding 24 hours, and exposure to environmental interference. Despite these constraints, the system demonstrates feasibility for real-time ECG monitoring with effective noise suppression performance. Nevertheless, further enhancements are necessary for clinical-grade deployment, including validation using annotated ECG datasets, the adoption of adaptive or hybrid filtering techniques, comprehensive evaluation under long-term ambulatory conditions, and quantitative assessment of system reliability metrics such as data integrity and power efficiency. Future work will prioritize integrating machine learning-based arrhythmia detection to further enhance diagnostic robustness and clinical applicability.

5. CONCLUSION

This study developed and evaluated a computationally efficient ECG denoising framework based on an IIR Butterworth filter for real-time IoT-based Holter monitoring systems. The results demonstrate that the proposed method effectively suppresses both low-frequency motion artifacts and high-frequency EMG interference, achieving statistically significant SNR improvements of 9.47 ± 1.96 dB for motion artifacts ($t(9) = 15.28$, $p < 0.001$) and 16.73 ± 0.91 dB for muscle artifacts ($t(9) = 58.11$, $p < 0.0001$). Quantitative error analysis shows that the filtering process yields a mean MSE of 0.006 and RMSE of 0.077 for motion artifacts, and a mean MSE of 0.008 and RMSE of 0.089 for muscle artifacts, indicating low signal distortion after filtering. Furthermore, post-filtering Pearson correlation exceeded 0.93 for all respondents (mean $r = 0.963$ for motion artifacts, $r = 0.945$ for muscle artifacts),

confirming that the proposed approach preserves clinically relevant ECG waveform morphology while substantially improving signal quality. These results collectively demonstrate that the method achieves an effective balance between noise reduction, signal fidelity, and real-time computational efficiency.

The proposed rule-based arrhythmia detection system achieved a post-filtering mean accuracy of 95.3% ± 2.1% (sensitivity: ≈96.0%, specificity: ≥97.0%, F1-score: ≥95.0%), which is statistically significantly greater than the 70% minimum clinical screening threshold ($t(9) = 29.7$, $p < 0.001$). This represents a meaningful improvement over the pre-filtering accuracy of 86.7%, demonstrating that noise reduction directly translates into enhanced arrhythmia detection reliability. Nevertheless, this validation is limited to threshold-based classification on a small, homogeneous dataset and does not constitute full clinical validation against annotated ECG databases or real-world patient populations.

Several limitations must be acknowledged. First, the dataset consists of only ten male subjects, which limits statistical robustness and reduces generalizability to broader populations, including female subjects and patients with clinically confirmed arrhythmias. Second, the absence of annotated clinical datasets prevents comprehensive validation of diagnostic performance against established benchmarks. Third, while all post-filtering correlation values exceeded 0.93, residual morphological distortion particularly under EMG noise suppression may still affect the interpretation of subtle waveform features in demanding clinical contexts. Fourth, the use of a rule-based arrhythmia detection approach limits classification capability compared to advanced machine learning methods. Finally, the experimental protocol was conducted under controlled short-duration conditions and does not fully represent long-term ambulatory monitoring scenarios, including continuous 24–48 hour recordings and varying environmental noise conditions.

The findings of this study have practical implications for the development of low-cost, real-time, and energy-efficient wearable ECG monitoring systems. By providing a practical balance between computational efficiency and signal quality enhancement, the proposed approach offers a promising candidate solution for embedded Holter devices, particularly in resource-constrained settings. Ultimately, this work contributes to advancing scalable and accessible cardiac monitoring technologies. However, the potential to support early detection of arrhythmias and improve preventive cardiovascular healthcare is contingent upon further validation using clinically annotated datasets and heterogeneous patient populations, including female subjects and individuals with confirmed cardiac conditions.

Acknowledgements

We would like to thank the Director of Poltekkes Kemenkes Surabaya for supporting and funding this research, as stated in the employment contract of the Director of SK. Hk.01.02/1/1905/2022. So that we can complete this research well and smoothly, and students who are involved and help with research hopefully can increase their knowledge and experience.

References

Addison, P. S. (2005). Wavelet transforms and the ECG: a review. *Physiological Measurement*, *26*(5), R155–R199. https://doi.org/10.1088/0967-3334/26/5/R01

Afaq Ahmad, Muhammad Lais, Dawar Awan, Muhammad Zia, Muhammad Uzair Khan, & Esha Farooq. (2025). ECG Denoising Using Wavelet Transform and Wiener Filter. *Physical Education, Health and Social Sciences*, *3*(3), 97–105. https://doi.org/10.63163/jpehss.v3i3.685

Ali, M. A., Ali, S., & Khorsheed, A. (2023). ECG Signal Denoising Using Discrete Wavelet Transform. *Journal of University of Duhok*, *26*(2), 450–463. https://doi.org/10.26682/sjuod.2023.26.2

Basu, S., & Mamud, S. (2020). Comparative Study on the Effect of Order and Cut off Frequency of Butterworth Low Pass Filter for Removal of Noise in ECG Signal. *2020 IEEE 1st International Conference for Convergence in Engineering (ICCE)*, 156–160.

https://doi.org/10.1109/ICCE50343.2020.9290646
Bhavna Soni Pritaj Yadav. (2025). Review of Hybrid Deep Learning Techniques For Robust ECG Signal Classification by Addressing Noise and Class Imbalance. *IITM Journal of Management and IT*, 63–79. https://doi.org/10.65301/iitm.2025.17.2.926
Bing, P., Liu, W., Zhai, Z., Li, J., Guo, Z., Xiang, Y., He, B., & Zhu, L. (2024). A novel approach for denoising electrocardiogram signals to detect cardiovascular diseases using an efficient hybrid scheme. *Frontiers in Cardiovascular Medicine*, *11*. https://doi.org/10.3389/fcvm.2024.1277123
Chatterjee, S., Thakur, R. S., Yadav, R. N., Gupta, L., & Raghuvanshi, D. K. (2020). Review of noise removal techniques in ECG signals. *IET Signal Processing*, *14*(9), 569–590. https://doi.org/10.1049/iet-spr.2020.0104
Clifford, G. D., Behar, J., Li, Q., & Rezek, I. (2012). Signal quality indices and data fusion for determining clinical acceptability of electrocardiograms. *Physiological Measurement*, *33*(9), 1419–1433. https://doi.org/10.1088/0967-3334/33/9/1419
Das, M., & Sahana, B. C. (2022). Deep-Learning-Based Approach for Automatic Detection and Correction of Ecg Artifacts. *SSRN Electronic Journal*. https://doi.org/10.2139/ssrn.4308281
Das, M., & Sahana, B. C. (2025). Optimized Orthogonal Wavelet-Based Filtering Method for Electrocardiogram Signal Denoising. *Journal of The Institution of Engineers (India): Series B*, *106*(3), 965–978. https://doi.org/10.1007/s40031-022-00796-6
Enayati, M., Farahani, N. Z., & Skubic, M. (2020). Machine Learning Approach for Motion Artifact Detection in Ballistocardiogram Signals. *Proceedings of the 14th EAI International Conference on Pervasive Computing Technologies for Healthcare*, 406–410. https://doi.org/10.1145/3421937.3421970
Galdos, J., Lopez Colque, N., Medina Rodirguez, A., Huarca Quispe, J., Rendulich, J., & Sulla Espinoza, E. (2024). Comparison and evaluation of LMS-derived algorithms applied on ECG signals contaminated with motion artifact during physical activities. *Applied Computer Science*, *20*(1), 157–172. https://doi.org/10.35784/acs-2024-10
Ghaleb, F. A., Kamat, M. B., Salleh, M., Rohani, M. F., & Abd Razak, S. (2018). Two-stage motion artefact reduction algorithm for electrocardiogram using weighted adaptive noise cancelling and recursive Hampel filter. *PLOS ONE*, *13*(11), e0207176. https://doi.org/10.1371/journal.pone.0207176
Hoffmann, J., Mahmood, S., Fogou, P. S., George, N., Raha, S., Safi, S., Schmailzl, K. J., Brandalero, M., & Hubner, M. (2020). A Survey on Machine Learning Approaches to ECG Processing. *2020 Signal Processing: Algorithms, Architectures, Arrangements, and Applications (SPA)*, 36–41. https://doi.org/10.23919/SPA50552.2020.9241283
Hou, Y., Liu, R., Shu, M., Xie, X., & Chen, C. (2023). Deep Neural Network Denoising Model Based on Sparse Representation Algorithm for ECG Signal. *IEEE Transactions on Instrumentation and Measurement*, *72*, 1–11. https://doi.org/10.1109/TIM.2023.3251408
Jinseok Lee, McManus, D. D., Merchant, S., & Chon, K. H. (2012). Automatic Motion and Noise Artifact Detection in Holter ECG Data Using Empirical Mode Decomposition and Statistical Approaches. *IEEE Transactions on Biomedical Engineering*, *59*(6), 1499–1506. https://doi.org/10.1109/TBME.2011.2175729
Karacan, I., Topkara Arslan, B., Karaoglu, A., Aydin, T., Gray, S., Ungan, P., & Türker, K. S. (2023). Estimating and minimizing movement artifacts in surface electromyogram. *Journal of Electromyography and Kinesiology*, *70*, 102778. https://doi.org/10.1016/j.jelekin.2023.102778
Khalili, M., GholamHosseini, H., Lowe, A., & Kuo, M. M. Y. (2024). Motion artifacts in capacitive ECG monitoring systems: a review of existing models and reduction techniques. *Medical & Biological Engineering & Computing*, *62*(12), 3599–3622. https://doi.org/10.1007/s11517-024-03165-1
Lahmiri, S. (2014). Comparative study of ECG signal denoising by wavelet thresholding in empirical and variational mode decomposition domains. *Healthcare Technology Letters*,

1(3), 104–109. https://doi.org/10.1049/htl.2014.0073

Lazaro, J., Reljin, N., Hossain, M. B., Noh, Y., Laguna, P., & Chon, K. H. (2020). Wearable Armband Device for Daily Life Electrocardiogram Monitoring. *IEEE Transactions on Biomedical Engineering*, *67*(12), 3464–3473. https://doi.org/10.1109/TBME.2020.2987759

Lazeta, L., Markovic, I., & Simovic, V. (2021). IIR filters designed for comparison and minimum-order design exploration using Matlab. *2021 44th International Convention on Information, Communication and Electronic Technology (MIPRO)*, 875–879. https://doi.org/10.23919/MIPRO52101.2021.9596760

Li, H., & Boulanger, P. (2021). An Automatic Method to Reduce Baseline Wander and Motion Artifacts on Ambulatory Electrocardiogram Signals. *Sensors*, *21*(24), 8169. https://doi.org/10.3390/s21248169

Liu, J., Zhou, X., Liu, X., Wang, X., & Zhou, J. (2023). A Rhythm-Specific ECG Signal Quality Assessment Framework for Robust Cardiac Health Monitoring of AI-based Arrhythmia Classifer. *2023 IEEE Biomedical Circuits and Systems Conference (BioCAS)*, 1–5. https://doi.org/10.1109/BioCAS58349.2023.10388946

Ma, M., Du, M., Feng, Q., & Xiahou, S. (2024). A new particle filter algorithm filtering motion artifact noise for clean electrocardiogram signals in wearable health monitoring system. *Review of Scientific Instruments*, *95*(1). https://doi.org/10.1063/5.0153241

Mahdavi, M. (2024). Complex-Domain FIR Filter Design for Signal Processing Applications. *2024 IEEE 22nd Mediterranean Electrotechnical Conference (MELECON)*, 180–185. https://doi.org/10.1109/MELECON56669.2024.10608765

Malleswari, P. N., Hima Bindu, Ch., & Satya Prasad, K. (2021). An Improved Denoising of Electrocardiogram Signals Based on Wavelet Thresholding. *Journal of Biomimetics, Biomaterials and Biomedical Engineering*, *51*, 117–129. https://doi.org/10.4028/www.scientific.net/JBBBE.51.117

Mohd Apandi, Z. F., Ikeura, R., Hayakawa, S., & Tsutsumi, S. (2020). An Analysis of the Effects of Noisy Electrocardiogram Signal on Heartbeat Detection Performance. *Bioengineering*, *7*(2), 53. https://doi.org/10.3390/bioengineering7020053

Mohguen, W., & Bouguezel, S. (2021). Denoising the ECG Signal Using Ensemble Empirical Mode Decomposition. *Engineering, Technology & Applied Science Research*, *11*(5), 7536–7541. https://doi.org/10.48084/etasr.4302

Pandey, V. K. (2010). Adaptive filtering for baseline wander removal in ECG. *Proceedings of the 10th IEEE International Conference on Information Technology and Applications in Biomedicine*, 1–4. https://doi.org/10.1109/ITAB.2010.5687642

Reddy, V. V., M.Neelaveni, M.Sandeep, Ahmad, Sk. K., & Krishna, P. V. (2023). Comparison of FIR and IIR filters using ECG signal with different sampling frequencies. *International Research Journal of Modernization in Engineering Technology and Science*. https://doi.org/10.56726/IRJMETS35977

S, S., & Sharma, R. (2025). Wavelets and multiresolution processing: theory and applications in signal and image analysis. *ICTACT Journal on Image and Video Processing*, *16*(1), 3641–3646. https://doi.org/10.21917/ijivp.2025.0514

Saha, S., & Barman Mandal, S. (2024). FPGA implementation of IIR elliptic filters for de-noising ECG signal. *Biomedical Signal Processing and Control*, *96*, 106544. https://doi.org/10.1016/j.bspc.2024.106544

Sharma, V. (2024). Design and Implementation of Efficient IIR Low Pass Filter Based On Vedic Multiplier Algorithm. *International Journal for Research in Applied Science and Engineering Technology*, *12*(1), 115–117. https://doi.org/10.22214/ijraset.2024.57881

Shen, J., Li, X., Wang, Y., Li, Y., Bian, J., Zhu, X., He, X., & Li, J. (2024). Anti-Motion Interference Electrocardiograph Monitoring System: A Review. *IEEE Sensors Journal*, *24*(10), 15727–15747. https://doi.org/10.1109/JSEN.2024.3383872

Skoric, J., D'Mello, Y., & Plant, D. V. (2024). A Wavelet-Based Approach for Motion Artifact Reduction in Ambulatory Seismocardiography. *IEEE Journal of Translational*

Engineering in Health and Medicine, *12*, 348–358. https://doi.org/10.1109/JTEHM.2024.3368291

Steinberg, J. S., Varma, N., Cygankiewicz, I., Aziz, P., Balsam, P., Baranchuk, A., Cantillon, D. J., Dilaveris, P., Dubner, S. J., El-Sherif, N., Krol, J., Kurpesa, M., La Rovere, M. T., Lobodzinski, S. S., Locati, E. T., Mittal, S., Olshansky, B., Piotrowicz, E., Saxon, L., … Piotrowicz, R. (2017). 2017 ISHNE-HRS expert consensus statement on ambulatory ECG and external cardiac monitoring/telemetry. *Heart Rhythm*, *14*(7), e55–e96. https://doi.org/10.1016/j.hrthm.2017.03.038

Vanchak, V., & Melnychuk, S. (2024). Discrete wavelet transform denoising method efficiency evaluation for processing pulse signals with harmonic components. *Scientific Journal of the Ternopil National Technical University*, *116*(4), 124–134. https://doi.org/10.33108/visnyk_tntu2024.04.124

WHO. (2025, July 31). Cardiovascular diseases (CVDs). *WHO*. https://www.who.int/news-room/fact-sheets/detail/cardiovascular-diseases-(cvds)

Xie, X., Liu, H., Shu, M., Zhu, Q., Huang, A., Kong, X., & Wang, Y. (2021). A multi-stage denoising framework for ambulatory ECG signal based on domain knowledge and motion artifact detection. *Future Generation Computer Systems*, *116*, 103–116. https://doi.org/10.1016/j.future.2020.10.024

Zeppenfeld, K., Tfelt-Hansen, J., de Riva, M., Winkel, B. G., Behr, E. R., Blom, N. A., Charron, P., Corrado, D., Dagres, N., de Chillou, C., Eckardt, L., Friede, T., Haugaa, K. H., Hocini, M., Lambiase, P. D., Marijon, E., Merino, J. L., Peichl, P., Priori, S. G., … Slade, A. (2022). 2022 ESC Guidelines for the management of patients with ventricular arrhythmias and the prevention of sudden cardiac death. *European Heart Journal*, *43*(40), 3997–4126. https://doi.org/10.1093/eurheartj/ehac262

BIOGRAPHIES OF AUTHORS

Sumber studied Engineering Physics (S2) Master of Technology Institute Sepuluh Nopember Surabaya from 2012-2014, as a lecturer in diagnostics, electrical installations and discrete electronics practicum at the Department of Electromedical Technology, Health Polytechnic, Ministry of Health, Surabaya. Other Tridarma activities carried out are carrying out community service activities and carrying out research activities. The current research is an analysis of the effectiveness of digital filters on electronic stethoscopes using the MAX 9814 sensor to diagnose heart conditions through heart sounds produced and detected by the stethoscope. Currently he is still an active member of Indonesian Electromedical Association (IKATEMI). This organization aims to increase the professionalism of electromedical and medical technology technicians in Indonesia. He can be contacted at email: Sumber72@poltekkesdepkes-sby.ac.id.

Endang Dian Setioningsih studied post-graduate studies in Electrical Engineering (S2) at the Sepuluh Nopember Institute of Technology, Surabaya. Graduated in 2010, as a lecturer teaching physics and therapeutic equipment courses in the Applied Undergraduate Study Program in Electro-medical Technology Engineering, Department of Electromedical Technology, Health Polytechnic, Ministry of Health, Surabaya. Other Tridarma activities carried out include carrying out community service activities as well as carrying out research activities. The current research is about wireless electronic stethoscopes.Research is also focused on sending sound signals and utilizing digital filters as one of the parameters to make research better. Currently he is also still active as a member of IndonesianElectromedical Association (IKATEMI). This organization aims to increase the professionalism of electromedical and medical technology technicians in Indonesia. Currently
also active as an administrator of Indonesian Electro-medical Personnel Education Association(APTEMI). She can be contacted at email: dian18@poltekkesdepkes-sby.ic.id.

Triwiyanto received the B.S. degree in Physics from Airlangga University, Indonesia, M.S. degrees in Electronic Engineering from the Institut Teknologi Sepuluh Nopember Surabaya, Indonesia in 2004, and the Ph.D. degree in Electrical Engineering from Gadjah Mada University, Yogyakarta, Indonesia, in 2018. From 1998 to 2004, he was a Senior Lecturer with the Microcontrollers Laboratory. Since 2005, he has been an Assistant Professor with the Medical Electronics Technology Department, Health Polytechnic Ministry of Health Surabaya, Indonesia. In 2018, Triwiyanto received the best Doctoral Student award from Gadjah Mada University. Additionally, he is Editor-in-chief in several peer review journals, Chairman and Technical Programme Committee in several International Conferences. His current research interests include microcontroller, electronics, biomedical signal processing, machine learning, rehabilitation engineering, and surface electromyography (sEMG)-based physical human robot interactions. He can be contacted at email: triwiyanto123@gmail.com.

Roichatun Nashichah received the S.Tr.TEM. degree in Electromedical Engineering from Health Polytechnic Ministry of Health Surabaya, Indonesia, in 2017, and the M.T. degree in Biomedical Engineering from Airlangga University, Surabaya, Indonesia, in 2022. Since 2025, she has been a Lecturer (Assistant Expert) with the Department of Electromedical Engineering, Health Polytechnic Ministry of Health Surabaya, Indonesia. Currently she is also still active as a member of Indonesian Electromedical Association (IKATEMI). This organization aims to increase the professionalism of electromedical and medical technology technicians in Indonesia. Currently
Her current research interests include) signal processing and dental laser (dentolaser) applications. She can be contacted at email: roichatun.nashicha@poltekkes-surabaya.ac.id

Professor Dr **Vijay Anant Athavale** was awarded PhD in Computer Science 2003 from Barkatullah University, Bhopal, India. He has a rich teaching, research and administrative experience of more than 34 years. He has served in Government and Private Universities and Colleges in India and abroad. He has served academic assignments at Canada, the Republic of Yemen and the Republic of Sudan. He has served as an expatriate expert for the United Nations Development Programme to Ethiopia. He has been instrumental in shaping of several Institutions of repute offering Technical and Management Education in India. He spearheaded many innovative initiatives including the industry academic integration and internationalization. As a thought leader and a subject-matter expert, he has presented numerous sessions at Conferences, FDPs, and Workshops and his work has been cited in over 690 publications